



# Experimental and numerical study of a new adjustable frictional damper



Hamid Rahmani Samani, Masoud Mirtaheri <sup>\*</sup>, Amir Peyman Zandi

Department of Civil Engineering, K.N. Toosi University of Technology, Tehran, Iran

## ARTICLE INFO

### Article history:

Received 16 August 2013

Accepted 13 May 2015

Available online xxxx

### Keywords:

Frictional damper

Energy dissipation

Passive control

Semi-active control

Hysteretic loading

## ABSTRACT

In this paper, the concept of a semi active frictional damper called Adjustable Frictional Damper (AFD) is introduced. The clamping force of such damper is secured by hydraulic pressure, which not only reduces the manufacturing costs but also makes it possible to control the seismic response of the structure by changing the clamping force of the dampers.

The hysteretic behavior of AFD is studied by experimental means as well as by numerical model. Experimental process involves tests with various hydraulic pressures (which cause various frictional forces) at nearly static loading as well as dynamic loading with various frequencies. The results show that the proposed damper has significant energy absorption by stable hysteretic loops, which can be used for enhancement of the performance of structures subjected to earthquake loads with various intensities. Force–displacement characteristics of AFD such as slippage load, dissipated energy, effective stiffness and equivalent viscous damping for consecutive cycles of loading is calculated. The system is qualified based on the requirements for displacement-dependent devices according to ASCE/SEI 41-06 specification. Furthermore, the hysteretic behavior of AFD is studied by numerical method and a close agreement between the experimental and numerical results is observed.

© 2015 Elsevier Ltd. All rights reserved.

## 1. Introduction

Seismic response control techniques involve addition of devices to the system in order to dissipate the energy imparted by earthquake motion (for a survey of such techniques see e.g. [1–4]). Frictional based dampers are one class of such devices which dissipate the energy through frictional mechanism caused by two solid bodies sliding relative to each other. A conventional frictional damper compromises a frictional sliding contact surface and a clamping mechanism that produces normal contact force on the surface and heavily relies on coefficient of friction between surfaces. In a passive frictional damper, the clamping force of the damper and consequently the slippage force is a pre-determined constant value selected by design. If the axial force in the damper which is usually placed in a bracing system overcomes the static frictional force, the passive damper starts to slip and a considerable amount of mechanical energy can be transformed to heat energy and dissipated.

Many different types of passive frictional energy dissipation devices have been developed and tested for seismic applications in recent years, and more are still being investigated. Pall and Marsh [5] proposed frictional dampers installed at the crossing joint of the X-brace. Tension

in one of the braces forces the joint to slip thus activating four links, which in turn force the joint in the other brace to slip. This device is usually called the Pall frictional damper. Wu et al. [6] introduced an improved Pall frictional damper (IPFD), which replicates the mechanical properties of the Pall frictional damper, but offers some advantages in terms of ease of manufacture and assembly. Sumitomo friction damper [7] utilizes a more complicated design. The pre-compressed internal spring exerts a force that is converted through the action of inner and outer wedges into a normal force on the friction pads. Fluor Daniel Inc. has developed and tested another type of frictional device which is called Energy Dissipating Restraint (EDR) [8]. The design of this friction damper is similar to the Sumitomo friction damper since this device also includes an internal spring and wedges encased in a steel cylinder. The EDR utilizes steel and bronze friction wedges to convert the axial spring force into normal pressure on the cylinder. A full description of the EDR mechanical is given in [9]. Constantine et al. [10] proposed frictional dampers composed of a sliding steel shaft and two frictional pads clamped by high strength bolts. Mualla and Belev [11] proposed a friction damping device and carried out tests for assessing the friction pad material. Habib Saeed Monir and Keyvan Zeynali [12] introduced and tested a modified friction damper (MFD) which is similar to pall friction damper however it is applied in the diagonal bracing. Recently Mirtaheri et al. [13] proposed an innovative type of frictional damper called cylindrical friction damper (CFD). In contrast with other frictional dampers the CFDs use shrink fit mechanism in lieu of high-strength bolts to induce friction between contact surfaces. This reduces construction costs, simplifies design computations and increase reliability in comparison with other types of frictional dampers.

<sup>\*</sup> Corresponding author at: K.N. Toosi University of Technology, Department of Civil Engineering, No. 1346, Valiasr St., Mirdamad intersection 19967, P.O. Box. 15875-4416, Tehran, Iran.

E-mail addresses: samani@dena.kntu.ac.ir (H.R. Samani), mmirtaheri@kntu.ac.ir (M. Mirtaheri), zandi@kntu.ac.ir (A.P. Zandi).

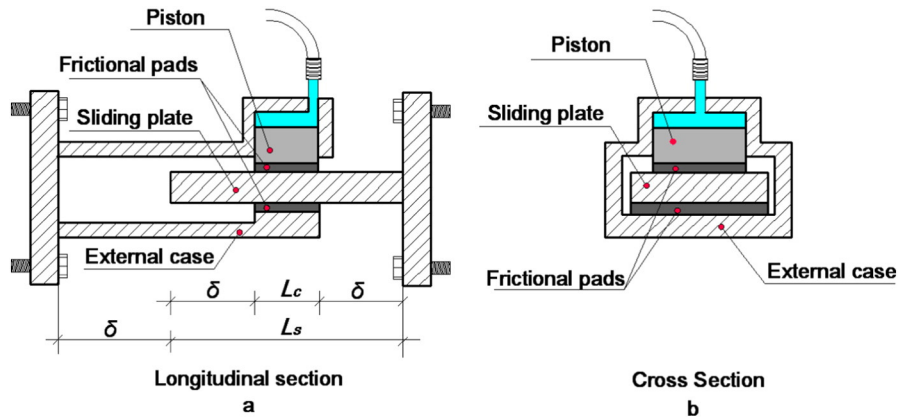


Fig. 1. Schematic view of AFD; a. longitudinal section; b. Cross section.

However, a frictional damper is not able to dissipate energy unless slippage force is exceeded. When the damper is not slipping, it has no advantage over a regular bracing member. So in high probable seismic events and if activating forces are overestimated in design the system cannot benefit from the added damping. The concept of semi-active control can be utilized to improve the efficiency of frictional dampers. A semi-active friction damper can adapt its slippage threshold during earthquake excitation according to structural responses in a smart fashion. Akbay and Aktan [14] were the pioneers in this field by introducing Active Slip Bracing Device (ASBD). The device allows the brace to axially elongate or contract through slippage when the brace loads reach the slippage force, which is controlled by a hydraulic actuator. Gaul and Nitsche [15] proposed semi-active joint connections in which piezoelectric stack disk is used as a washer to control in real time the normal force in the friction interface of joints based on feedback from sensor outputs. If a voltage is applied to the piezoelectric washer, the stack disk tends to expand, which results in increasing the normal force and slippage threshold. Chen et al. [16] introduced piezoelectric friction damper (PFD). The clamping force in such a damper is regulated by piezoelectric actuators. However, piezoelectric based frictional dampers are not applicable to building structures due to the fact that the force produced by a piezoelectric actuator is rather small in value. Moreover piezoelectric actuators are not cost effective. Agrawal and Yang [17] proposed an electromagnetic frictional damper. This device is based on the regulation of friction force across the damper using electromagnetic field. Similar to piezoelectric ones, activating force of electromagnetic based devices can also produce forces which are rather small in value.

In this investigation, the hysteretic behavior of a semi-active type of frictional damper called the Adjustable Frictional Damper (AFD) is studied experimentally and numerically. The clamping force of such damper is secured by hydraulic pressure. The advantage of AFD is the fact that it

is capable of producing large forces. In terms of construction costs, this system is more cost effective.

First of all, the hysteretic behavior of AFD is studied experimentally with various hydraulic pressures causing different slippage forces at the rate of 0.1 Hz which is nearly considered static. The results show that the proposed damper has significant energy absorption by stable hysteretic loops, which can improve the performance of structures subjected to earthquake loads with various intensities. Force–displacement characteristics of AFD such as slippage load, dissipated energy, effective stiffness and equivalent viscous damping for consecutive cycles of loading are found by test and calculated by standard methods. Also, dynamic loading of the device is conducted at various frequencies to assess the effects of dynamic loading on the response of AFD for possibility of decay of slippage force. The hysteretic behavior of AFD is also studied by numerical method. The results of numerical model closely correlate with experimental results.

## 2. Components and mechanism of adjustable frictional damper

The mechanism of AFD is similar to a car braking system. This damper consists of three main parts; external case, piston and sliding plate. As



Fig. 2. AFD prototype.



Fig. 3. Test setup.

**Table 1**  
Specification of static test cases.

Test case	Hydraulic pressure (bar)	Area of piston (mm <sup>2</sup> )	Stroke	Frequency of loading (Hz)
Case A	100	1962.5	± 40mm	0.1
Case B	130	1962.5	± 40mm	0.1
Case C	190	1962.5	± 40mm	0.1

shown in Fig. 1 the clamping force is secured by the hydraulic pressure exerted on the piston. The hydraulic pressure is provided by a mechanical or even hydroelectric pump. The pressure can be easily changed at little energy expense, so the device can be classified as semi active.

**3 . AFD design computations**

The AFD can be conveniently set for different slippage loads by selecting the appropriate geometric parameters and hydraulic pressure. For simplicity, all parameters except hydraulic pressure, *P* can be considered to be constant, and the desired slippage load can be set by changing the value for *P*. This leads to typical and more economic

construction of the dampers. This means that all dampers are uniformly manufactured and then are adjusted for the design pressure necessary to induce required frictional force for the structure. The slippage force of the damper can be calculated as follow

$$F_s = 2\mu PA_p \tag{1}$$

where *A<sub>p</sub>* is the cross-sectional area of the piston, *μ* is friction coefficient and *P* is the hydraulic pressure. The procedure for designing the AFD starts with determining maximum slippage load *F<sub>s</sub>* and maximum displacement of dampers *δ* by structural analysis of the models including trial dampers, or an equivalent damping for the damped structure.

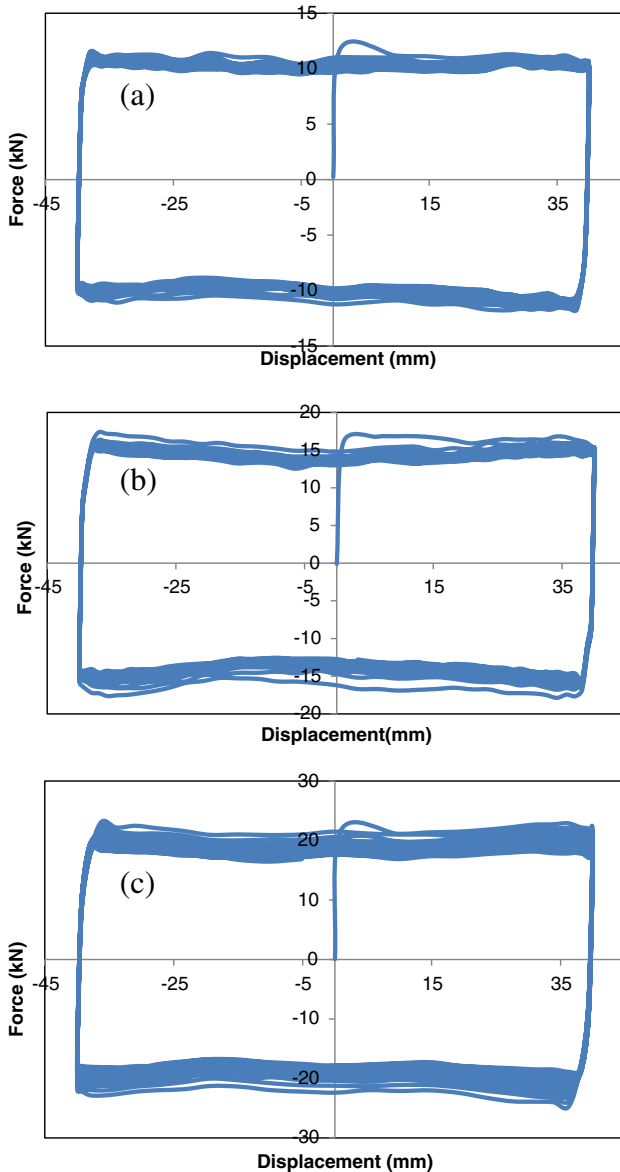


**Fig. 4.** Experimental hysteretic force–displacement curve of AFD: (a) case A; (b) case B; (c) case C.

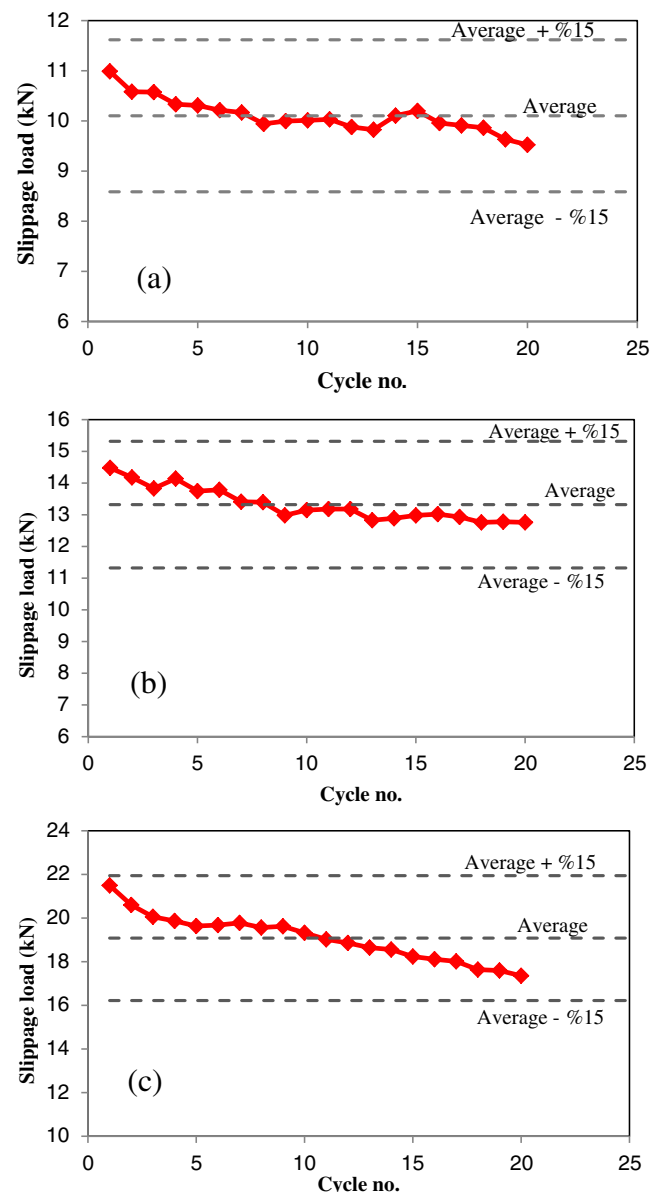


**Fig. 5.** Slippage load versus cycle number: (a) case A; (b) case B; (c) case C.

**Table 2**  
Slippage load, effective stiffness and dissipated energy for each cycle of loading (case A).

Cycle no.	Slippage load (kN)	Deviation from average	Effective stiffness (kN/m)	Deviation from average	Dissipated energy (J)	Deviation from average
1	10.99	8.80	259.035	3.931	1728.12	7.34
2	10.58	4.77	254.345	2.049	1702.52	5.75
3	10.57	4.70	254.247	2.010	1683.61	4.57
4	10.33	2.30	248.336	-0.361	1663.90	3.35
5	10.31	2.07	253.466	1.696	1653.20	2.68
6	10.21	1.14	254.443	2.088	1636.93	1.67
7	10.17	0.67	254.345	2.049	1628.83	1.17
8	9.94	-1.57	255.22	2.402	1608.48	-0.09
9	10.00	-1.03	249.166	-0.028	1605.06	-0.31
10	10.01	-0.88	253.173	1.578	1603.32	-0.41
11	10.03	-0.68	252.782	1.422	1593.92	-1.00
12	9.88	-2.19	248.873	-0.146	1587.33	-1.41
13	9.82	-2.73	246.430	-1.126	1582.05	-1.74
14	10.11	0.05	251.414	0.8732	1586.43	-1.46
15	10.20	0.98	238.858	-4.164	1578.18	-1.98
16	9.96	-1.42	239.102	-4.066	1581.82	-1.75
17	9.91	-1.88	241.740	-3.007	1570.43	-2.46
18	9.86	-2.35	243.352	-2.361	1566.52	-2.70
19	9.63	-4.63	240.763	-3.400	1563.68	-2.88
20	9.52	-5.71	245.649	-1.439	1493.94	-7.21
Average	10.10		249.2377		1610.9135	

Proper material for the sliding plate and frictional pad may be selected by specifying a certain  $\mu$ . By these values geometric dimensions, i.e.  $A_p$  may be selected and the hydraulic pressure can be computed by Eq. (1).

#### 4. Experimental study of hysteretic behavior of the AFD

Uniaxial tests are performed to determine the axial force displacement curve of the AFD. The tests are conducted at displacements below the extreme value for lockout of the damper. The protocol for the testing of the AFD is based on the requirements for displacement-dependent devices according to ASCE/SEI 41-06 [18]. Twenty full displacement cycles are applied to the specimen. The experimental testing included both dynamic and static loading. Firstly, the hysteretic behavior of AFD is studied under three different hydraulic pressures at a rate of 0.1 Hz (statically). Secondly, dynamic testing of the device is conducted at different frequencies as will be described in Section 4.4. The frictional pads and sliding plate are not replaced during the tests.

**Table 3**  
Slippage load, effective stiffness and dissipated energy for each cycle of loading (case B).

Cycle No.	Slippage load (kN)	Deviation from average	Effective stiffness (kN/m)	Deviation from average	Dissipated energy (J)	Deviation from average
1	14.48	8.70	401.56	11.25	2546.50	13.38
2	14.18	6.44	382.90	6.08	2429.03	8.15
3	13.83	3.83	372.42	3.18	2331.87	3.83
4	14.14	6.16	387.63	7.39	2385.13	6.20
5	13.75	3.20	358.74	-0.61	2334.60	3.95
6	13.79	3.51	373.97	3.61	2299.14	2.37
7	13.41	0.67	374.01	3.62	2261.38	0.69
8	13.40	0.58	373.40	3.45	2235.76	-0.45
9	12.98	-2.53	363.09	0.60	2213.28	-1.45
10	13.15	-1.30	361.09	0.04	2202.02	-1.95
11	13.18	-1.05	366.99	1.68	2182.96	-2.80
12	13.18	-1.05	366.07	1.42	2169.93	-3.38
13	12.83	-3.70	340.98	-5.53	2169.00	-3.42
14	12.89	-3.25	352.29	-2.48	2160.00	-3.83
15	12.98	-2.55	345.40	-4.42	2161.20	-3.77
16	13.02	-2.25	348.18	-3.59	2158.60	-3.89
17	12.93	-2.93	341.12	-5.53	2155.21	-4.04
18	12.76	-4.20	339.78	-6.08	2151.90	-4.19
19	12.78	-4.05	336.16	-6.91	2148.60	-4.33
20	12.76	-4.20	335.86	-7.19	2143.50	-4.56
Average	13.32		361.082		2241.98	

**Table 4**  
Slippage load, effective stiffness and dissipated energy for each cycle of loading (case C).

Cycle no.	Slippage load (kN)	Deviation from average	Effective stiffness (kN/m)	Deviation from average	Dissipated energy (J)	Deviation from average
1	21.49	12.54	430.64	10.99	3446.98	13.21
2	20.60	7.85	429.84	10.78	3330.40	9.38
3	20.06	5.01	415.96	7.21	3240.09	6.42
4	19.87	4.03	421.24	8.57	3177.30	4.35
5	19.63	2.80	420.36	8.34	3117.81	2.40
6	19.68	0.01	414.84	6.92	3078.84	1.12
7	19.78	5.66	411.35	6.02	3145.74	3.32
8	19.57	2.44	407.31	4.98	3152.81	3.55
9	19.62	2.74	391.82	0.99	3114.55	2.29
10	19.32	1.17	392.64	1.20	3081.12	1.19
11	19.02	-0.40	393.62	1.45	3042.48	-0.07
12	18.86	-1.26	379.36	-2.23	3016.62	-0.92
13	18.65	-2.38	369.56	-4.75	2981.06	-2.09
14	18.56	-2.85	363.66	-6.27	2954.34	-2.97
15	18.24	-4.53	359.20	-7.42	2917.11	-4.19
16	18.11	-5.17	360.53	-7.08	2885.25	-5.24
17	18.01	-5.69	356.27	-8.18	2857.49	-6.15
18	17.64	-7.66	350.48	-9.67	2834.13	-6.92
19	17.60	-7.88	347.75	-10.37	2807.02	-7.81
20	17.35	-9.14	343.36	-11.51	2649.42	-12.98
Average	19.08		387.99		3041.53	

#### 4.1. AFD prototype fabrication process

AFD is very similar to an automobile disk braking system. For this matter, the prototype initial model is based on an actual braking system of a typical automobile as shown in Fig. 2. The external case is made of cast iron and the sliding plate is made of structural mild steel conforming to ASTM A36. The diameter of the piston is 48 mm. Width and thickness of the sliding plate is 55 and 6 mm respectively. The frictional pads are made of semi-metallic materials. Pads are approximately rectangular with dimensions of 78.8 × 40 mm and thickness of 13.5 mm. The coefficients of static and dynamic frictions ( $\mu_s, \mu_k$ ) are obtained based on several tests being 0.307 for  $\mu_s$  and 0.286 for  $\mu_k$ .

#### 4.2. Test setup

AFD specimen is tested in a universal testing machine in vertical position as shown in Fig. 3. The testing machine has a capacity of 300 kN and 500 mm of travel. The testing machine is equipped with an internal Linear Variable Displacement Transducer (LVDT) and 980 kN load cell in line with the cylinder. The force-displacement relationship for each cycle of each test was recorded by the data acquisition system.

#### 4.3. Static loading

In this section the hysteretic behavior of AFD is achieved under three different hydraulic pressures at the rate of 0.1 Hz which is nearly static. The specifications of these three tests are shown in Table 1. All tests are performed on a single specimen. The frictional pads and sliding plate are not replaced during the tests.

The hysteretic axial force-displacement curves for Cases A to C described previously in Table 1 are presented in Fig. 4. As one could expect, the AFD exhibits classical rectangular hysteresis loops. Furthermore, the AFD has almost the same performance in compression and tension. The temperature of the sliding plate after the last cycle is measured to be about 80, 90 and 120 °C for the cases A, B and C respectively.

##### 4.3.1. Qualification of force-displacement characteristics

**4.3.1.1. Slippage force.** The slippage loads for any single cycle are calculated as the maximum force at zero displacement. Fig. 5 presents the

**Table 5**  
Specification of dynamic test cases.

Test case	Hydraulic pressure (bar)	Area of piston (mm <sup>2</sup> )	Stroke	Frequency of loading (Hz)
Case D	70	1962.5	± 20mm	0.5
Case E	70	1962.5	± 20mm	0.7
Case F	70	1962.5	± 20mm	1

slippage load versus number of cycles for cases A to C. As can be seen, slippage load is decreased over the cycles. However, this reduction is within the acceptable range according to ASCE/SEI 41-06 requirements for a prototype displacement based energy dissipation device. The specification requires that within each test, the slippage force does not differ by more than plus or minus 15% from the average value of slippage load as calculated from all cycles in that test. Tables 2 to 4 also compare the slippage load of each cycle of loading with the average value for test cases A to C respectively. The maximum deviation from average is related to the first cycle of the case C and is equal to 12.54%.

**Table 6**  
Slippage load for each cycle of dynamic loading.

Cycle no.	Case D (0.5 Hz)		Case E (0.7 Hz)		Case F (1 Hz)	
	Slippage load (kN)	Deviation from average	Slippage load (kN)	Deviation from average	Slippage load (kN)	Deviation from average
1	8.27364	14.90412	7.8947	17.3302	7.1016	8.614562
2	7.56652	5.083634	7.1680	6.530693	6.7539	3.296707
3	7.05864	-1.96976	7.1758	6.646816	6.4726	-1.00538
4	7.54308	4.758085	7.1837	6.762939	6.8164	4.252731
5	7.42587	3.13039	6.8946	2.466371	6.6914	2.340694
6	6.89456	-4.24854	6.7539	0.376138	6.7070	2.579697
7	7.41025	2.913354	7.0196	4.324348	6.3476	-2.91742
8	7.28523	1.177136	6.3867	-5.08168	6.5117	-0.40788
9	7.03520	-2.2953	6.5820	-2.17858	6.7930	3.894215
10	7.08208	-1.64421	6.8633	2.001879	6.6719	2.041929
11	6.98832	-2.94638	6.6445	-1.24959	6.6133	1.145667
12	7.44150	3.347406	6.5351	-2.87532	6.5586	0.309145
13	7.02739	-2.40381	6.3242	-6.01066	6.2929	-3.75393
14	6.94144	-3.59747	6.6289	-1.48184	5.9101	-9.60956
15	7.28523	1.177136	6.7070	-0.3206	6.3476	-2.91742
16	7.06645	-1.86125	6.5664	-2.41083	6.6758	2.101691
17	6.94144	-3.59747	6.7070	-0.3206	6.3007	-3.63442
18	6.69922	-6.96139	6.2070	-7.75252	6.6602	1.862677
19	7.09771	-1.4272	6.3320	-5.89453	6.6289	1.38467
20	7.12115	-1.10165	6.8399	1.6535	6.3476	-2.91742
21	7.14459	-0.77611	6.4765	-3.74626	6.6094	1.085916
22	7.08208	-1.64421	6.5195	-3.10757	6.2851	-3.87343
23	7.19928	-0.01652	6.3476	-5.66229	6.2851	-3.87343
Average	7.20047		6.7286		6.5384	

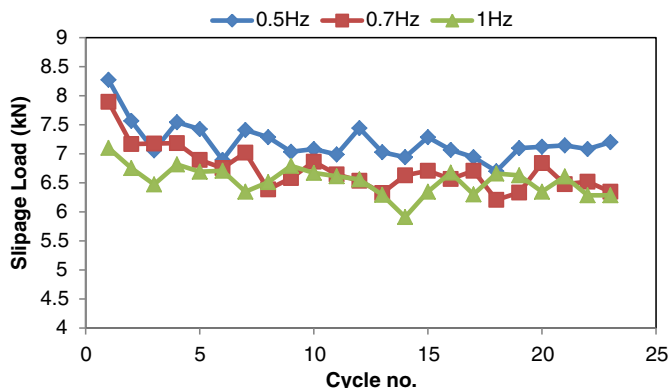


Fig. 6. Slippage load versus cycle number for different frequencies.

4.3.1.2. *Effective stiffness.* For linear analysis of friction damped structures, the frictional damper system can be represented by an equivalent linear elastic model with an effective stiffness such calibrated to characterize the inherent nonlinear properties. Therefore, it is of interest to find an effective stiffness  $K_{eff}$  for AFDs.

The effective stiffness of a friction based energy dissipation device can be calculated from test data as follows:

$$K_{eff} = \frac{|F^+| + |F^-|}{|\Delta^+| + |\Delta^-|} \quad (2)$$

where the forces in the specimen,  $F^+$  and  $F^-$ , are evaluated at maximum displacements  $\Delta^+$  and  $\Delta^-$  respectively.

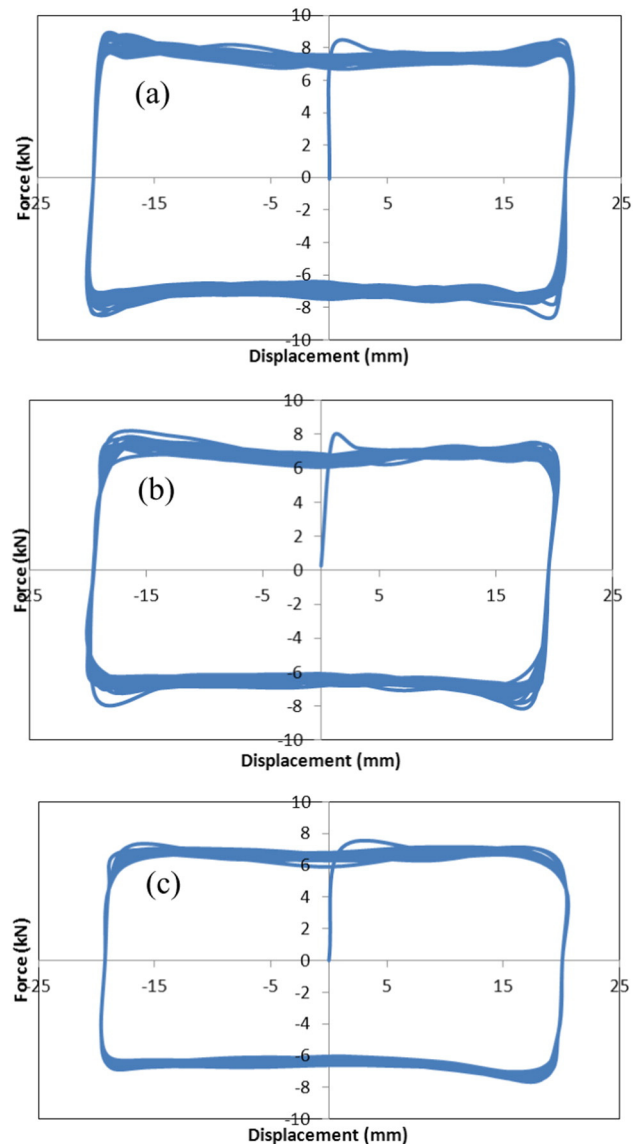


Fig. 7. Experimental hysteretic force–displacement curve of AFD: (a) case D; (b) case E; (c) case F.

Similar to slippage force, ASCE/SEI 41-06 specification requires that within each test, the effective stiffness of a displacement based prototype energy dissipation device for any one cycle does not differ by more than plus or minus 15% from the average effective stiffness as calculated from all cycles in that test. Tables 2 to 4 compare the effective stiffness of each cycle of loading to the average for test cases A to C respectively.

**4.3.1.3. Dissipated energy.** The dissipated energy in each cycle,  $W_D$ , shall be taken as the area enclosed by one complete cycle of the force displacement response. The area of the hysteresis loop ( $W_D$ ) of a prototype energy dissipation device for any one cycle must not differ by more than plus or minus 15% from the average. The dissipated energy of each cycle of loading is presented in Tables 2 to 4 for test cases A to C respectively. As can be seen, the maximum deviation from the average belongs to the very first cycle of the case C which is 13.38%.

#### 4.4. Dynamic loading

In order to evaluate the effects of dynamic loading, the specimen is tested under three different frequencies of 0.5 Hz, 0.7 Hz and 1 Hz as shown in Table 5. Each test includes 23 full displacement cycles applied to the specimen. Due to the limitations of the testing machine, the stroke is taken as 20 mm and hydraulic pressure as 70 bars. The slippage load value of each cycle of loading and its deviation from average is shown in Table 6. As can be seen, neglecting the first cycle of case E, that is frequency of 0.7 Hz, the deviation from average for all the cycles of each test is less than 15%. Fig. 6 displays the slippage load versus

number of cycles. The hysteretic force–displacement curves of the cases D to F are shown in Fig. 7. Once again these curves present a classic rectangular hysteresis loops.

The average value of slippage load decreases to somewhat, as the frequency of loading is increased; this is due to brake fade which is caused by the heat generated in the contact surfaces. However, when the frequency is increased from 0.5 Hz to 1 Hz, the average slippage load is decreased %9.

## 5. Numerical study of hysteretic behavior of the AFD

### 5.1. Mechanical analysis

A three dimensional finite element model of the prototype device is developed as shown in Fig. 8(a). 20-node brick solid elements are used to model the sliding plate and the frictional pads as well as the piston. Surface to surface contact is utilized to simulate the friction between the piston and the upper pad and also between the sliding plate and pads. As the first step of the analysis, relevant value of hydraulic pressure is applied to the piston. Fig. 8(b) shows the resulting von mises stress for the case A. Secondly, a cyclic displacement with the stroke similar to experimental load is applied to the model. The resulting force displacement curves are obtained. For the purpose of comparison between experimental setup and numerical model the hysteretic curves are superimposed on each other as shown in Figs. 9 and 10. As can be seen there is a close agreement between the numerical results and those obtained by experiments.

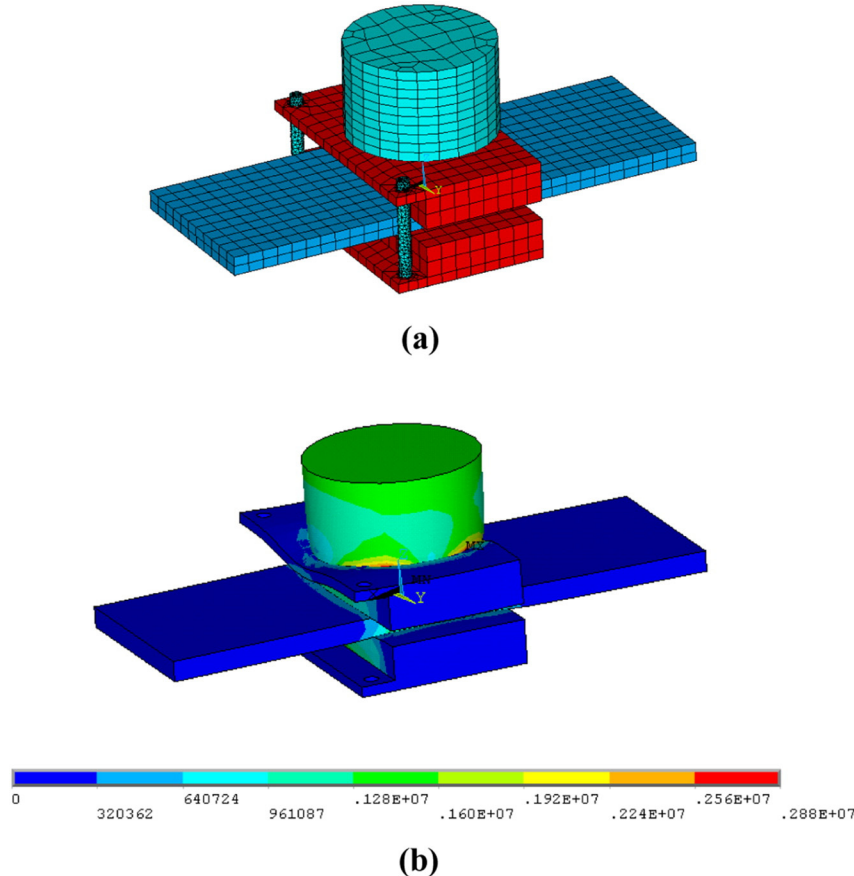


Fig. 8. (a) Finite element model of AFD. (b) Von-mises stress developed after the first step of analysis for the case A (Pa).

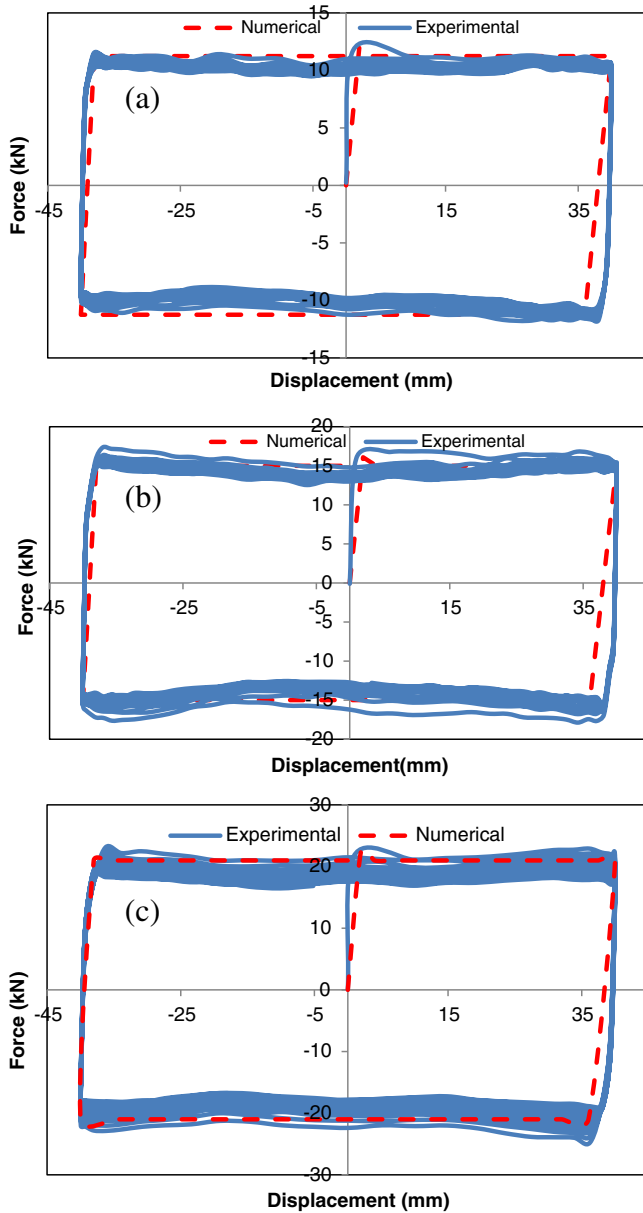


Fig. 9. Comparison between numerical and experimental force–displacement curves: (a) case A; (b) case B; (c) case C.

## 5.2. Thermal analysis

The rate of heat generation due to friction  $\dot{W}_D$ , between contact surfaces is calculated as follows:

$$\dot{W}_D = v \times F_s \quad (3)$$

where  $v$  is the relative velocity between the sliding plates and braking pads and  $F_s$  is the slippage force. Replacing Eq. (1) into Eq. (3) leads to:

$$\dot{W}_D = 2v\mu P A_p. \quad (4)$$

Some of this frictional heat is absorbed by the sliding plate and the rest is absorbed by the pads that is:

$$\dot{W}_D = \dot{W}_{DS} + \dot{W}_{DP} = \gamma \dot{W}_D + (1-\gamma) \dot{W}_D. \quad (5)$$

The terms  $\dot{W}_{DS}$  and  $\dot{W}_{DP}$  are the amount of absorbed heat by the sliding plate and the pads, respectively.  $\gamma$  is the dimensionless coefficient of

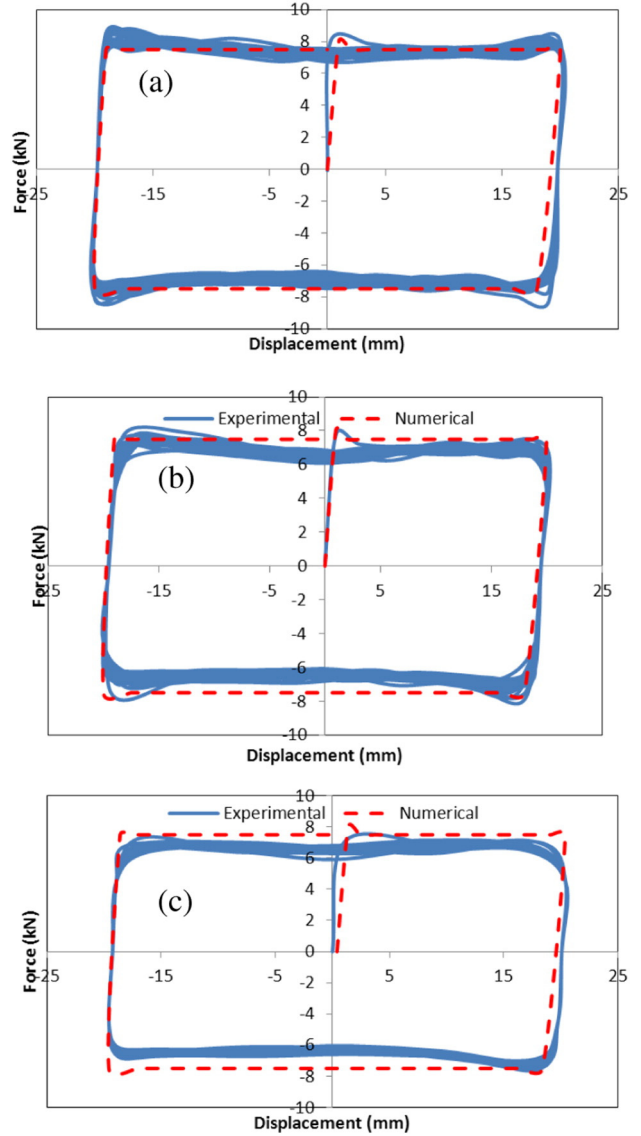


Fig. 10. Comparison between numerical and experimental force–displacement curves: (a) case D; (b) case E; (c) case F.

heat partitioning. For a perfect contact condition  $\gamma$  can be considered as 0.5 [19]. The heat flux into the frictional pad  $q_p$ , and sliding plate (on each side)  $q_s$ , is calculated as the rate of thermal energy divided by the contact surface area as follows:

$$q_p = \frac{\dot{W}_{DP}}{S_c} = (1-\gamma) \frac{v \times F_s}{2 \times S_c} = (1-\gamma) \frac{v\mu P A_p}{S_c} \quad (6)$$

$$q_s = \frac{\dot{W}_{DS}}{S_c} = \gamma \frac{v \times F_s}{2 \times S_c} = \gamma \frac{v\mu P A_p}{S_c} \quad (7)$$

where  $S_c$  is the contact surface area. In order to assess the temperature change of the sliding plate over the time in different test cases, a moving heat flux is applied to the model at the contact length as shown in Fig. 11 and its value is calculated by Eq. (7). The assumptions for transient thermal analysis are given in Table 7. Note that the geometry and element sizes of the sliding plate for thermal analysis is similar to the one used for mechanical analysis (Fig. 8). However, the elements are replaced by thermal ones.

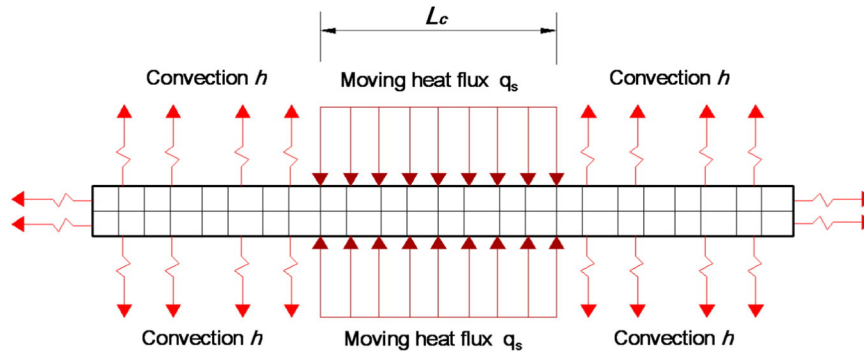


Fig. 11. Thermal loading of the sliding plate.

Table 7

Assumptions for transient thermal analysis.

Conductivity (w/m <sup>2</sup> ·k)	Density (kg/m <sup>3</sup> )	Specific heat (J/kg·k)	Convection coefficient, h (w/m <sup>2</sup> ·k)	Ambient temperature (°C)
44	7850	460	60	20

Fig. 12 shows the temperature of the sliding plate after 20 cycles. The average temperature from finite element model matches the temperature measured during the test.

### 6. Equivalent viscous damping

It is of interest to provide a frictional damper with a damping index by which it can be quantified upon design and calculations. An equivalent viscous damping index is defined by Chopra [20] to determine the damping coefficient for structural members. This coefficient is

equivalent in some sense to the combined effect of damping mechanisms present in an actual structure and is defined by Eq. (8):

$$\beta_{eff} = \frac{1}{2\pi} \frac{W_D}{k_{eff} \Delta_{ave}^2} \tag{8}$$

$\Delta_{ave}$  is equal to the average of the absolute values of displacements  $\Delta^+$  and  $\Delta^-$ .

It should be mentioned that this equivalent damping index is an idealization and is quite approximate for nonlinear systems [20]. However,

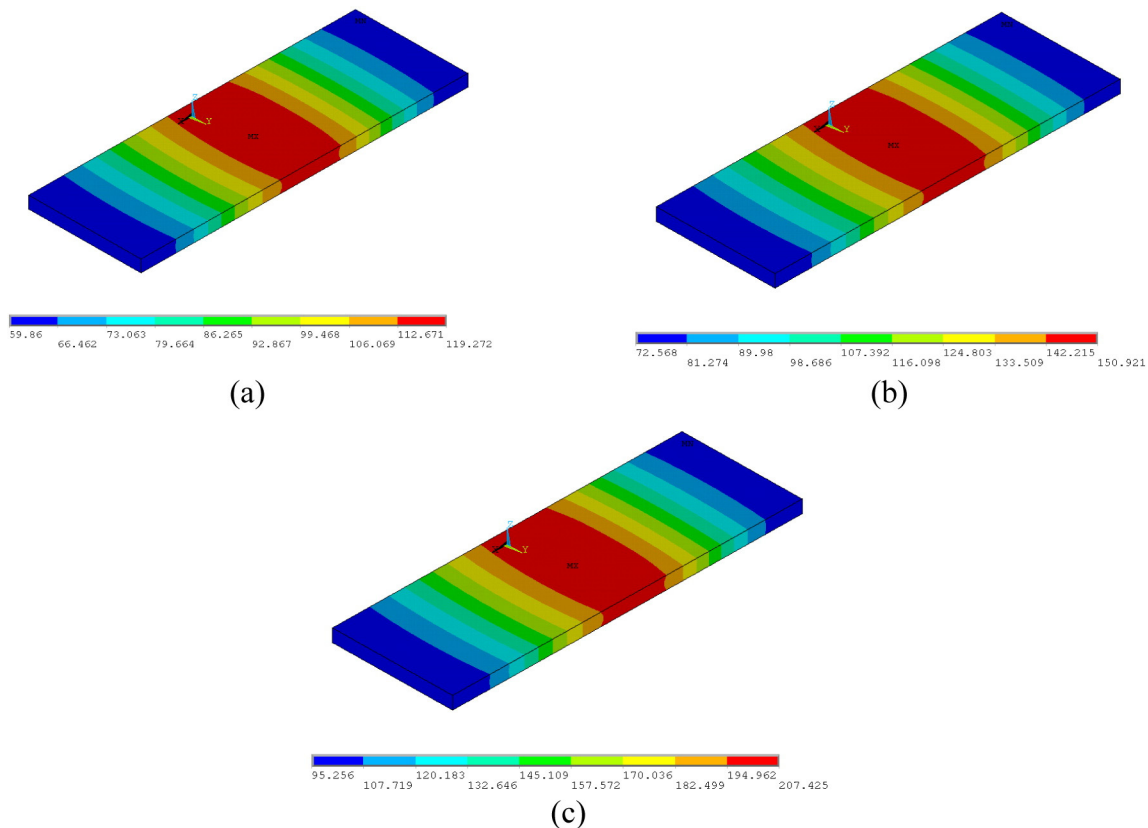


Fig. 12. Temperature of the sliding plate after 20 cycles; (a) case A; (b) case B; (c) case C.

**Table 8**  
Equivalent viscous damping.

Cycle no.	Case A	Case B	Case C
1	0.664	0.631	0.652
2	0.666	0.631	0.630
3	0.659	0.623	0.596
4	0.666	0.612	0.595
5	0.649	0.647	0.625
6	0.640	0.612	0.623
7	0.637	0.601	0.598
8	0.627	0.596	0.629
9	0.641	0.606	0.595
10	0.630	0.607	0.617
11	0.627	0.592	0.614
12	0.634	0.590	0.619
13	0.639	0.633	0.617
14	0.628	0.610	0.620
15	0.657	0.623	0.623
16	0.658	0.617	0.628
17	0.646	0.629	0.625
18	0.640	0.631	0.624
19	0.646	0.636	0.621
20	0.605	0.636	0.590
Average	0.643	0.618	0.617

it incorporates both stiffness and energy dissipation per cycle and may be used as an equivalent damping index in an approximate sense. Calculating this damping index for all cycles, an average damping index could be provided for each Case (Table 8). The equivalent viscous damping is particularly useful for linear dynamic analyses.

## 7. AFD as a passive damper

As previously mentioned, most of frictional dampers are made of a set of steel plates with certain friction coefficient that are forced by bolt pretension in order to induce the friction between the involved elements. Using pre-tensioned bolts to induce friction, makes the behavior of frictional dampers unpredictable. The relaxation or loosening of the link elements such as spring or bolts contributes to this unpredictability and may lead to decay of slippage load. AFD may also be utilized as a passive damper as long as the hydraulic pressure and thus the friction, is kept at a constant value. In this case the slippage load of AFD can be conveniently evaluated by measuring the hydraulic pressure and compensated if required. Another important advantage of AFD is that re-centering is no longer a concern. Although the device can be utilized as a reliable passive damper, its pressure can be easily changed such that with minimum time delay the system is converted to a semi-active system.

## 8. Conclusions

A semi-active frictional damper which is called Adjustable Frictional Damper (AFD) was introduced. The clamping force of such damper is secured by hydraulic pressure. Unlike other kinds of semi-active frictional dampers, AFDs are applicable to building structures and they are more cost effective because of easy manufacturing and low

maintenance. Another important advantage of AFD is that re-centering is no longer a concern.

Experimental studies of AFD show that the performance of the device is predictable since it is quite easy to measure the hydraulic pressure and also reliable since decay of slippage load over the cycles is in an acceptable range of ASCE/SEI 41-06 specification. The force–displacement characteristics of AFD such as slippage load, dissipated energy, effective stiffness and equivalent viscous damping for consecutive cycles of loading were calculated and qualified based on the requirements of the ASCE/SEI 41-06 specification. The effects of dynamic loading (various frequencies) also were considered. Similar behavior as static loading was observed. Numerical model which simulates the test conditions was constructed and studied. Close agreement in terms of hysteretic force–displacement curve was achieved.

## References

- [1] M. Mirtaheeri, A. Gheidi, A.P. Zandi, P. Alanjari, H. Rahmani Samani, Experimental optimization studies on steel core lengths in buckling restrained braces, *J. Constr. Steel Res.* 67 (8) (2011) 1244–1253.
- [2] A.A. Golafshani, A. Gholizad, Friction damper for vibration control in offshore steel jacket platforms, *J. Constr. Steel Res.* 65 (1) (2009) 180–187.
- [3] Hongwei Ma, Yam Michael C.H., Modelling of a self-centring damper and its application in structural control, *J. Constr. Steel Res.* 67 (4) (2011) 656–666.
- [4] H.H. Khoo, C. Clifton, J. Butterworth, G. MacRae, S. Gledhill, G. Sidwell, Development of the self-centering sliding hinge joint with friction ring springs, *J. Constr. Steel Res.* 78 (2012) 201–211.
- [5] A.S. Pall, C. Marsh, Response of friction damped braced frames, *J Struct Eng ASCE* 108 (9) (1982) 1313–1323.
- [6] B. Wu, J. Zhang, M.S. Williams, J. Oua, Hysteretic behavior of improved Pall-typed frictional dampers, *Eng. Struct.* 27 (2005) 1258–1267.
- [7] I.D. Aiken, J.M. Kelly, Earthquake Simulator Testing and Analytical Studies of Two Energy-Absorbing Systems for Multi-Story Structures. Report No. UCB/EERC-90/03, Earthquake Engineering Research Center, University of California, Berkeley (CA), 1990.
- [8] D.K. Nims, et al., Application of the energy dissipating restraint to buildings, *Proc. ATC 17-1 on seismic isolation, energy dissipation and active, control* 1993, pp. 627–638.
- [9] T.T. Soong, G.F. Dargush, *Passive energy Dissipation Systems in Structural Engineering*, John Wiley & Sons, New York, 1997.
- [10] M.C. Constantinou, A. Mokha, A.M. Reinhorn, Teflon bearings in base isolation, II: modeling, *J Struct Eng ASCE* 116 (2) (1990) 455–474.
- [11] I.H. Mualla, B. Belev, Performance of steel frames with a new friction damper device under earthquake excitation, *Eng. Struct.* 24 (3) (2002) 365–371.
- [12] H.S. Monir, K. Zeynali, A modified friction damper for diagonal bracing of structures, *J. Constr. Steel Res.* 87 (2013) 17–30.
- [13] M. Mirtaheeri, A.P. Zandi, S.S. Samadi, H. Rahmani Samani, Numerical and experimental study of hysteretic behavior of cylindrical friction dampers, *Eng. Struct.* 33 (2011) 3647–3656.
- [14] S. Kannan, H.M. Uras, H.M. Aktan, Active control of building seismic response by energy dissipation, *Earthq. Eng. Struct. Dyn.* 24 (1995) 747–759.
- [15] L. Gaul, H. Albrecht, J. Wirmitzer, Semi-active friction damping of large space truss structures, *Shock. Vib.* 11 (3) (2004) 173–186.
- [16] G. Chen, G.T. Garret, C. Chen, F.Y. Cheng, Piezoelectric friction dampers for earthquake mitigation of buildings: design, fabrication and characterization, *Struct. Eng. Mech.* 17 (2004) 539–556.
- [17] A. Agrawal, J. Yang, A semi-active electromagnetic friction damper for response control of structures, *Advanced Technology in Structural Engineering*, ASCE, Philadelphia 2000, pp. 1–8.
- [18] ASCE/SEI 41-06, *Seismic Rehabilitation of Existing Buildings*, American Society of Civil Engineers (ASCE), Reston (VA), 2006.
- [19] D. Majcherczak, P. Dufrenoy, M. Nait-Abdelaziz, Third body influence on thermal friction contact problems: application to braking, *J. Tribol.* 127 (2005) 89–95.
- [20] A.K. Chopra, *Dynamics of Structures: Theory and Applications to Earthquake Engineering*, 2nd ed. Prentice Hall, New Jersey, 2001..